24-GHz Impedance-Modulated BPSK Tags for Range Tracking and Vital Signs Sensing of Multiple Targets Using an FSK Radar

Jing Wang[®], Student Member, IEEE, Daniel Rodriguez[®], Graduate Student Member, IEEE, Ashish Mishra[®], Student Member, IEEE, Prateek Reddy Nallabolu, Graduate Student Member, IEEE, Tanja Karp[®], Senior Member, IEEE, and Changzhi Li[®], Senior Member, IEEE

Abstract—In this article, fully integrated binary phase shift keying (BPSK) tags are presented to work in conjunction with narrowband frequency-shift keying (FSK) radar for concurrent multitarget range tracking and vital signs sensing. Without the employment of any radio frequency (RF) mixer, the developed BPSK tag introduces a frequency offset by generating periodic phase shifts to the radar carrier frequencies with optimized power level. The theory of BPSK tag-based range tracking and vital signs sensing in conjunction with FSK radar signal is developed. An impedance-modulated 24-GHz tag architecture without any active RF components is proposed and its implementation and characterization are presented. The system performance is evaluated in the following residential indoor scenarios: single tag ranging, concurrent multiple tags and an untagged human target detection, and multiple tagged human targets tracking. Promising ranging performance demonstrates the potential for the proposed system to be adopted in various indoor tracking applications.

Index Terms—Binary phase shift keying (BPSK), frequency-shift keying (FSK) radar, identification and tracking, multiple targets, range tracking, vital signs sensing, wireless sensor.

I. Introduction

THE arising Internet of Things (IoT) era aims to link wearable sensors, everyday objects, and devices to the core Internet in a wireless manner for a human-centered environment. Contextual information, such as human location, activities, and surrounding objects, will be collected to realize context-aware computing. As the IoT market continues to grow, its key enabler, radio frequency identification (RFID) technology, has drawn increasing attention in recent years. RFID technology [1]–[5] uses radio waves to communicate between the tag and the reader. Radio frequency (RF) enabled identification and tracking approaches have the benefits of contactless, lightweight, and multitag sensing that do not

Manuscript received July 27, 2020; revised October 2, 2020; accepted October 28, 2020. Date of publication January 8, 2021; date of current version March 4, 2021. This work was supported by the National Science Foundation (NSF) under Grant ECCS-2030094, Grant 2028863, and Grant 1808613. (Corresponding author: Jing Wang.)

The authors are with the Department of Electrical and Computer Engineering, Texas Tech University (TTU), Lubbock, TX 79409 USA (e-mail: anna.wang@ttu.edu; daniel-fernando.rodriguez@ttu.edu; ashish.mishra@ttu.edu; prateek-reddy.nallabolu@ttu.edu; tanja.karp@ttu.edu; changzhi.li@ttu.edu).

Color versions of one or more figures in this article are available at https://doi.org/10.1109/TMTT.2020.3045201.

Digital Object Identifier 10.1109/TMTT.2020.3045201

require line-of-sight arrangements. While commercial RFID tags have been widely used in identifying objects and coarse-grained localization (i.e., when an object is in the proximity of the detector), they lack the ability to provide accurate location information of objects. Therefore, several customized RF tags have been proposed in the literature [6]–[17], which provide the capability to identify and track the location of the tagged humans or objects.

In general, these customized RF tags can be divided into two categories: passive and active. Passive tags do not require a power source (i.e., battery) to operate. Harmonic [6]-[10] and intermodulation tags [11]-[14] are both passive RF tags, which exploit the nonlinear properties of electronic components, such as diodes, transistors, and mixers, to differentiate the tag from natural clutters, such as furniture, walls, and plants, which do not exhibit nonlinear behaviors by detecting responses from the tags at the nonlinear frequency tones. However, harmonic tracking systems suffer from high path loss and signal licensing issues. Intermodulation systems require a costly hardware architecture in order to suppress the fundamental tones and amplify the intermodulation responses. Furthermore, both tracking approaches lack identification functionality, which means they cannot identify multiple tags simultaneously.

Conversely, active tags need a power source. Subharmonic tags [15] fall under the active tag category because they require the use of a frequency divider, mandating a power source. The subharmonic tracking sensor has lower path loss due to lower nonlinear frequency(s) compared with the harmonic one, when both operate at the same fundamental frequency. However, this advantage comes at the cost of larger receiver and tag sizes. A self-injection-locked (SIL) active tag was proposed in [16] for concurrent vital sign and location detection of multiple individuals. Note that the detection of "stationary" human subjects in that work was still based on the physiological motions of the target, e.g., through breathing and heartbeat. This motion-based sensing approach cannot detect completely stationary targets (i.e., motionless targets), which limits its applications. Moreover, due to clock synchronization protocol and mutual injection pulling issues in time division multiple access (TDMA) and code division multiple access (CDMA), frequency division multiple access (FDMA) was selected

0018-9480 © 2021 IEEE. Personal use is permitted, but republication/redistribution requires IEEE permission. See https://www.ieee.org/publications/rights/index.html for more information.

and implemented manually to simultaneously detect multiple subjects, adding operational complexity and cost. A switched injection-locked oscillator-based active backscatter tag was designed in [17] for frequency-modulated continuous-wave (FMCW) radar systems to improve range accuracy in dense multipath environments. However, FMCW radar [18]–[20] occupies a large bandwidth, which leads to high bandwidth requirements on system components and high spectrum usage. Significant expansion in wireless communications has led to a shortage in the available radio spectrum [21]. An identification and tracking system that occupies less bandwidth is thus preferred to tackle the spectrum shortage issue.

Narrowband frequency-shift keying (FSK) radar technology has been investigated in previous works [22]–[26] for Doppler frequency-based moving target tracking and vital signs-based stationary human target detection with much lower bandwidth usage than its wideband counterparts (e.g., FMCW radar). However, because the range detection mechanism is motion based, it lacks the ability to detect completely stationary targets. In addition, since the vital sign frequencies of multiple individuals tend to overlap, it is not reliable to sense vital sign information from multiple individuals, let alone vital signs-based multitarget tracking.

In this work, active binary phase shift keying (BPSK) tags are proposed to work in conjunction with an FSK radar for ubiquitous range tracking and motion sensing of multiple targets. Moreover, the BPSK tags enable detection and location of completely stationary objects even without any vibration or physiological motion. The proposed BPSK tag design shifts the phase of the carrier signals periodically, which is equivalent to generating a frequency offset to the carrier frequencies. By programming each BPSK tag with its own unique modulation frequency, multiple BPSK tags can be detected simultaneously based on their unique signature without any modification to the FSK radar reader or the employment of multiple access technology. In addition, unlike harmonic and subharmonic tags that require either two different antennas or a single antenna operating at two frequency bands, the impedancemodulated BPSK tag only needs one antenna designed for a single frequency band, thus reducing the tag size and design complexity. Furthermore, the BPSK tag utilization results in an intermediate frequency (IF) in the baseband, corresponding to the modulation frequency of the tag. Hence, low-frequency environmental noise can be avoided in motion sensing and its associated range tracking since the motion frequency is shifted to the vicinity of the low-IF [27]-[29]. The tradeoff is that the low-IF topology requires higher sampling rate and more computation resources for the radar reader. Nonetheless, low-cost high-speed off-the-shelf analog-to-digital converters (ADCs) and modern digital processors are readily available to meet such needs.

The BPSK tag-based range tracking and vital signs sensing theories are explained in Section II. BPSK tag design and implementation are presented in Section III. Various types of experiments are provided in Section IV. The advantages and limitations of the proposed system are discussed in Section V. Finally, conclusions are drawn in Section VI.

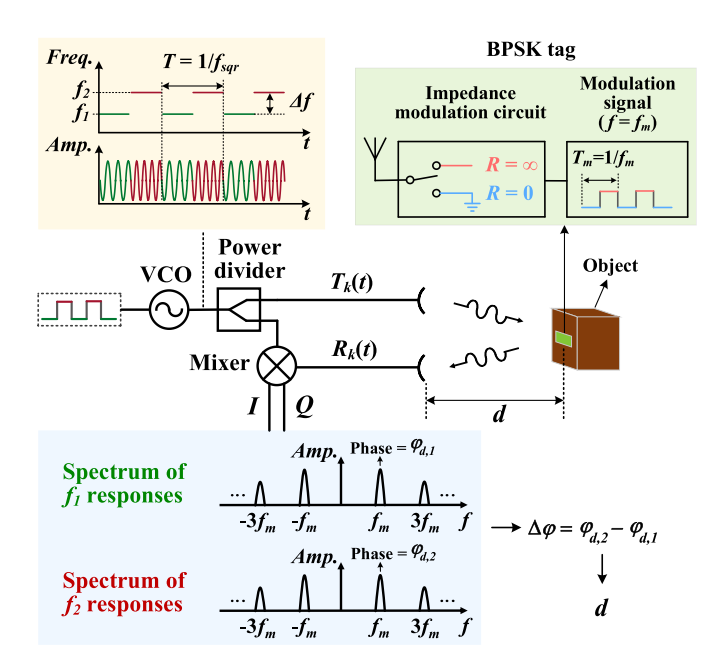


Fig. 1. Illustration of the proposed BPSK-tag-based range estimation of a tagged object.

II. FUNDAMENTAL THEORY

As shown in Fig. 1, in an FSK radar system, the transmit frequency is switched back and forth between two frequencies, f_1 and f_2 , at a switching rate of $f_{\rm sqr}$. The frequency shift between the two carriers, i.e., $\Delta f = f_2 - f_1$, is small, when being compared to the carrier frequencies. The transmit signal, neglecting the switching process between the two frequencies, can be represented as

$$T_k(t) = \cos(2\pi f_k t + \varphi_{o,k}(t)) \tag{1}$$

where k = 1, 2 and $\varphi_{o,k}(t)$ is the phase noise from the oscillator. Without loss of generality, the amplitudes of all signals are normalized to unity.

In BPSK modulation, the modulating signal m(t) is restricted to two amplitudes, which are here assumed to be $A = \pm 1$. Each amplitude introduces a constant phase shift to the carrier signal, resulting in the following modulated signal:

$$s(t) = \begin{cases} \cos(2\pi f_k t + \varphi_L), & \text{when } A = 1\\ \cos(2\pi f_k t + \varphi_H), & \text{when } A = -1. \end{cases}$$
 (2)

The difference between the two phase shifts is maximized and typically chosen as $\varphi_H - \varphi_L = 180^\circ$, which allows to interpret BPSK as double-sideband suppressed carrier modulation. Exploiting $\cos(\alpha + 180^\circ) = -\cos(\alpha)$ yields

$$s(t) = \begin{cases} \cos(2\pi f_k t + \varphi_L), & \text{when } A = 1\\ -\cos(2\pi f_k t + \varphi_L), & \text{when } A = -1. \end{cases}$$
 (3)

BPSK tag-based range tracking and vital signs monitoring will be analyzed in Sections II-A and II-B.

A. BPSK Tag-Based Range Tracking

The proposed BPSK tag alternates the phase of the carrier signal periodically by modulating the tag's impedance between

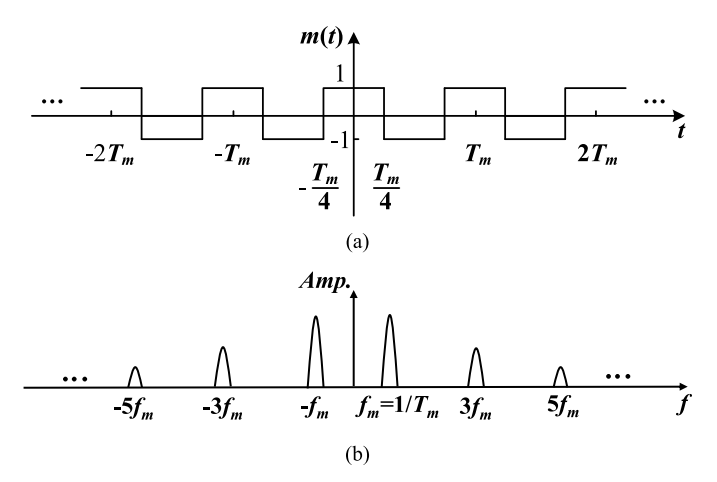


Fig. 2. Modulation signal of the BPSK tag. (a) Signal representation in the time domain. (b) Spectrum representation in the frequency domain.

two states: open circuit and short circuit. The modulating signal m(t) with a modulation frequency of $f_m = 1/T_m$ that is much smaller than the FSK switching rate $f_{\rm sqr}$ is shown in Fig. 2(a). It can be represented using Fourier expansion as

$$m(t) = \frac{4}{\pi} \sum_{n=1}^{\infty} \frac{1}{n} \sin\left(\frac{n\pi}{2}\right) \cos(2\pi n f_m t). \tag{4}$$

Note that only odd harmonic frequencies are present in (4). The BPSK tag is designed such that when m(t) = 1, it reflects the carrier signals with a phase offsets φ_L and when m(t) = -1 with $\varphi_H = \varphi_L + 180^\circ$. Thus, the received signal can be written as

$$R_k(t) = m(t)\cos\left[2\pi f_k t - \varphi_{d,k} - \varphi_L + \varphi_{o,k}\left(t - \frac{2d}{c}\right) - \varphi_{r,k}\right]$$
 (5)

where c is the speed of light, d represents the range to target at a particular time $t = t_0$, $\varphi_{d,k} = 4\pi d/\lambda_k$, λ_k is the wavelength corresponding to each carrier frequency, and $\varphi_{r,k}$ denotes the phase delay in the receiver circuit. Since $\varphi_{r,1}$ and $\varphi_{r,2}$ are normally very small and are very close to each other, they will be neglected in the following analysis. The received signals will be down converted using a copy of the transmit signal at the mixer to obtain the complex valued baseband output

$$B_k(t) \approx m(t) \exp[j(\varphi_{d,k} + \varphi_L + \varphi_k)]$$
 (6)

where $\varphi_k = \varphi_{o,k}(t) - \varphi_{o,k}(t-2d/c)$ is the total residual phase. According to range correlation theory [30], φ_k is very small compared to the phase delay term caused by the distance to the target and, hence, will be omitted from the following analysis. Applying Fourier expansion by substituting (4) into (6), the baseband signal equation becomes

$$B_k(t) \approx \frac{4}{\pi} \sum_{n=1}^{\infty} \frac{1}{n} \sin\left(\frac{n\pi}{2}\right) \cos(2\pi n f_m t) \exp\left[j\left(\varphi_{d,k} + \varphi_L\right)\right]$$
(7)

with Fourier transform

$$X_k(f) \approx \frac{2}{\pi} \sum_{n=1}^{\infty} \frac{1}{n} \sin\left(\frac{n\pi}{2}\right) e^{j(\varphi_{dk} + \varphi_L)} \times [\delta(f - nf_m) + \delta(f + nf_m)]. \quad (8)$$

Fig. 1 shows the modulation frequency and its odd number harmonics being part of the spectrum of both f_1 and f_2 responses. Though all the harmonics carry the same phase information for each carrier response spectrum, the phase information is sought at the fundamental tone pair for their highest signal-to-noise ratio (SNR) compared with the rest of the harmonic tones, assuming a white noise environment. The phase difference of the fundamental tone pair is calculated as

$$\Delta\varphi(t) = \varphi_{d,2} - \varphi_{d,1} = \frac{4\pi d}{\lambda_2} - \frac{4\pi d}{\lambda_1}.$$
 (9)

Range estimation can be derived accordingly as

$$d = \frac{c\,\Delta\varphi(t)}{4\pi\,\Delta f}.\tag{10}$$

Simultaneous identification and tracking of multiple tags are made possible by programming each tag with a unique modulation frequency. Individual ranges can be obtained by tracking the phase difference on the associated modulation frequency pairs for the tag of interest.

B. BPSK Tag-Based Multitarget Vital Signs Sensing and Range Detection

In an FSK radar system, where a stationary target of interest at nominal distance D has a periodic physiological body movement (i.e., respiration or heartbeat) that can be modeled as $x(t) = \mu \sin(2\pi f_0 t)$, with μ being the motion peak amplitude and f_0 the motion frequency, the radar signal will be reflected with its phase modulated by the time-varying physiological motion x(t) and a constant phase determined by D. The received signal is represented as [25]

$$R_k(t) = \cos\left(2\pi f_k t - \varphi_{x,k} - \varphi_{D,k} + \varphi_{o,k}\left(t - \frac{2D}{c}\right) - \varphi_{r,k}\right) \tag{11}$$

where $\varphi_{x,k} = 4\pi x(t) / \lambda_k$ and $\varphi_{D,k} = 4\pi D / \lambda_k$. Similarly, when a BPSK tag with a modulating signal m(t) is attached to the human target, additional periodic phase shifts of φ_L and φ_H are generated. The corresponding received signal is

$$R_{k}(t) = m(t)\cos\left(2\pi f_{k}t - \varphi_{x,k} - \varphi_{D,k} - \varphi_{L} + \varphi_{o,k}\left(t - \frac{2D}{c}\right) - \varphi_{r,k}\right).$$

$$(12)$$

As mentioned previously, the $\varphi_{r,k}$ term will be omitted. After the down-conversion, applying the range correlation effect, the complex-valued baseband output is obtained as

$$B_{k}(t) \approx m(t) \exp\left[j\left(\varphi_{x,k} + \varphi_{D,k} + \varphi_{L}\right)\right]$$

$$= m(t) \exp\left[j\left(\frac{4\pi x(t)}{\lambda_{k}} + \varphi_{D,k} + \varphi_{L}\right)\right]$$

$$= m(t) \exp\left[j\left(\frac{4\pi \mu \sin(2\pi f_{0}t)}{\lambda_{k}} + \varphi_{D,k} + \varphi_{L}\right)\right]$$

$$= m(t) \sum_{l=-\infty}^{\infty} J_{l}\left(\frac{4\pi \mu}{\lambda_{k}}\right) \exp\left[j\left(2\pi l f_{0}t + \varphi_{D,k} + \varphi_{L}\right)\right]$$
(13)

where the Bessel series approximation [31] was applied in the last step with J_l denoting the lth order Bessel function of

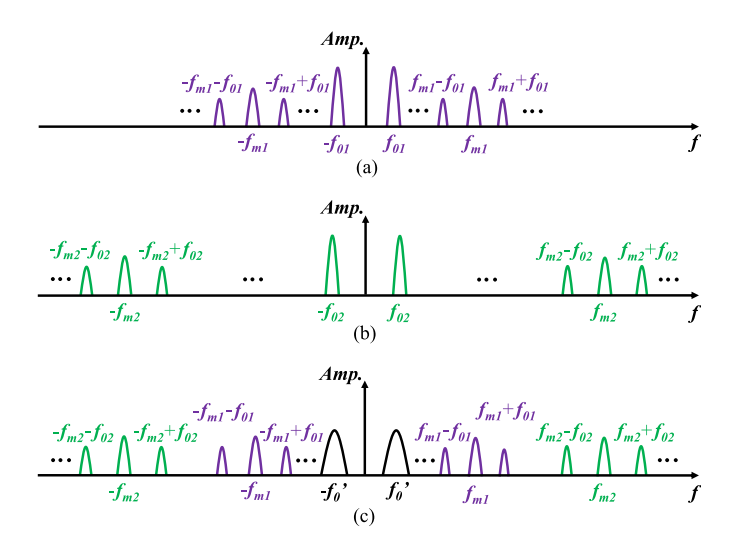


Fig. 3. Illustration of the spectra of BPSK-tag-based multihuman detection. (a) Spectrum when only tagged human target 1 is present. The corresponding modulation frequency is f_{m1} and vital sign frequency is f_{01} . (b) Spectrum when only tagged human target 2 is present. The corresponding modulation frequency is f_{m2} and vital sign frequency is f_{02} . (c) Spectrum when both targets are present. f_0' is the result of overlapping of f_{01} and f_{02} .

the first kind. Replacing m(t) by its Fourier series expansion results in

$$B_k(t) = \frac{4}{\pi} \sum_{n=1}^{\infty} \frac{1}{n} \sin\left(\frac{n\pi}{2}\right) \cos(2\pi n f_m t) \sum_{l=-\infty}^{\infty} J_l\left(\frac{4\pi \mu}{\lambda_k}\right) \times \exp\left[j\left(2\pi l f_0 t + \varphi_{D,k} + \varphi_L\right)\right]$$
(14)

with the following Fourier transform:

$$X_{k}(f) = \frac{2}{\pi} \sum_{n=1}^{\infty} \frac{1}{n} \sin\left(\frac{n\pi}{2}\right) \sum_{l=-\infty}^{\infty} J_{l}\left(\frac{4\pi \mu}{\lambda_{k}}\right) e^{j\left(\varphi_{D,k} + \varphi_{L}\right)} \times \left[\delta(f - nf_{m} - lf_{0}) + \delta(f + nf_{m} - lf_{0})\right].$$
(15)

As shown in Fig. 3(a) and (b), the vital sign frequency f_0 is modulated onto the tag's modulation frequency f_m , resulting in frequencies $nf_m \pm lf_0$ in the spectrum. The phase difference of any frequency peak pair is the same, which is

$$\Delta\varphi(t) = \frac{4\pi D}{\lambda_2} - \frac{4\pi D}{\lambda_1}.\tag{16}$$

Accordingly, the target range can be derived as

$$D = \frac{c \,\Delta \varphi(t)}{4\pi \,\Delta f}.\tag{17}$$

Though phase difference and range estimation can be calculated from the vital sign frequency pair, the results are susceptible to close proximity noise and interference. In addition, the vital sign frequencies of multiple individuals are likely to be similar. As can be seen from Fig. 3(c), since f_{01} and f_{02} are very close to each other, when both targets are present, their vital signs overlap and cannot be separated. Therefore, simultaneous multitarget vital sign sensing and its corresponding range estimation cannot be achieved from the f_0 pairs. In comparison, since BPSK tags are registered with different modulation frequencies (e.g., f_{m1} , f_{m2} , etc.), by finding the phase differences at known modulation frequencies or their related pairs (i.e., $nf_m \pm lf_0$, $n \neq 0$), concurrent multitarget vital

sign sensing and range detection can be accomplished. Note that Fig. 3 shows narrowband spectra instead of the spectral lines derived in (15), which assumed infinite length periodic signals. Finite observation time is modeled as windowing of the infinite length signal and results in the Fourier transform of the window function emerging at the location of the spectral lines.

Note that the modulation frequencies should be sufficiently separated, and the strongest modulation frequency-related pair should be selected to achieve the most reliable range detection performance.

C. Range Resolution

Range resolution is the ability of a radar system to distinguish between two adjacent targets. For FMCW radar, its range resolution depends on the carrier bandwidth. For a conventional FSK radar system, it does not have range resolution because it does not occupy a bandwidth. For the proposed BPSK tag-assisted FSK radar system, it possesses range resolution because it is capable of resolving closely spaced targets. However, the range resolution is largely determined by the successful detection of BPSK tags' modulation frequencies or their associated frequency products on the spectra, which is related to the selection of modulation frequencies and fast Fourier transform (FFT) window size.

If the BPSK tags' modulation frequencies are set apart enough so that there is no interference between the desired modulation frequency-related pairs and other frequency products, the tagged multiple targets can be successfully detected no matter how closely spaced they are. If the spectral leakages cause interferences, longer FFT window size can be used to reduce the spectral leakage, yet at the tradeoff of slower range update rate.

Therefore, the range resolution of the proposed system is determined by the selection of tags' modulation frequencies, the FFT window size, and the desired range update rate.

D. Modulation Frequency Selection

According to (8) and (15), besides the modulation frequencies, their odd number harmonics will also be present on the spectra. To avoid the interference between the modulation frequencies and the harmonics, the lowest modulation frequency should be set to more than one third of the highest modulation frequency. The rest of the modulation frequencies should be set in between with sufficient frequency separation. In this way, possible interference is avoided because all the harmonics will have higher frequencies than the modulation frequencies.

E. Maximum Unambiguous Range

Due to the periodicity of the sine wave, $\Delta \varphi(t)$ can only reach a maximum of 2π . Therefore, FSK radar has a maximum unambiguous range limitation of

$$R_{\text{max}} = \frac{c}{2\Delta f}.$$
 (18)

The maximum unambiguous range is inversely proportional to the frequency shift between the two carrier frequencies. Therefore, frequency shift can be reduced to accommodate higher maximum discernible range requirement at the tradeoff

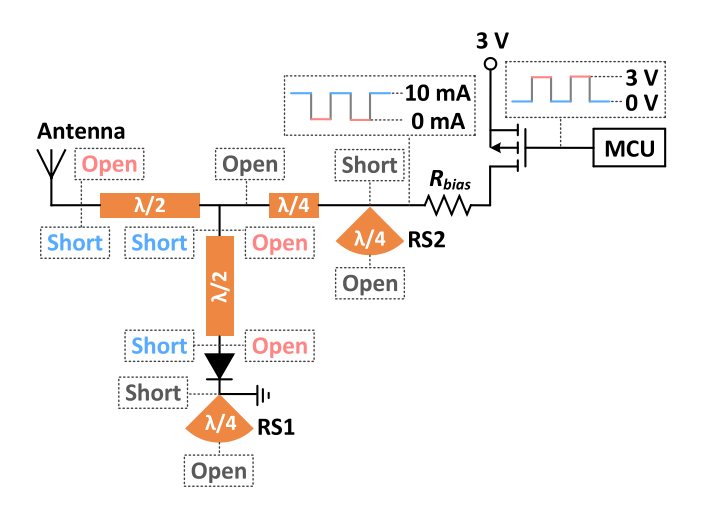


Fig. 4. Architecture of the BPSK tag design.

of reduced measurement precision. If measurement precision needs to be maintained while longer maximum unambiguous range is desired, a smart handover from period to period using a continuity constraint on the distance assisted by a reference system can be implemented [22]. The maximum unambiguous range can also be increased by utilizing more than two carriers [32] or modulating at least one of the carriers.

III. BPSK TAG DESIGN AND IMPLEMENTATION

In an FSK radar system, when the target is completely stationary, a Doppler shift is not applied to the radar signals, making the target reflections indistinguishable from the clutter response. Therefore, it is necessary to introduce a unique frequency offset, e.g., through BPSK modulation as discussed in Section II, to the stationary target response so that it can be separated from other stationary clutters. The most direct approach is upconverting the carrier signals using a mixer-based tag. However, RF mixers can be costly and/or power intensive. In addition, this type of architecture requires separate receive and transmit antennas at the cost of approximately twice the size of a single-antenna tag.

To implement a BPSK modulation without the involvement of an RF mixer, a backscatter tag with a variable reflection coefficient Γ is designed to periodically change the phase of the reflected signal. To maximize the strength of the reflected signal (i.e., reflecting the entire signal), the magnitude of Γ should be equal to one for any selected phase shift. Hence, short $(\Gamma=-1)$ and open $(\Gamma=1)$ circuits at the antenna port are desired so that ideally, when $\Gamma=-1$, all the carrier signals are reflected back with 180° phase shift; when $\Gamma=1$, all the carrier signals are reflected back with 0° phase shift.

The schematic of the proposed 24-GHz backscatter tag is depicted in Fig. 4. When the switching signal is in a low state, a 12-mA dc bias current flows through the pin diode to ground. The RF ground (i.e., short circuit) created by the radial stub RS1 is in parallel with the RF open created by the radial stub RS2 and the quarter-wave transformer. A half-wavelength transmission line is used to connect the pin diode to the rest of the structure and for the antenna connection. Conversely, when the switching signal is in a high state, the pin diode is reverse biased and thus no dc current will be flowing to

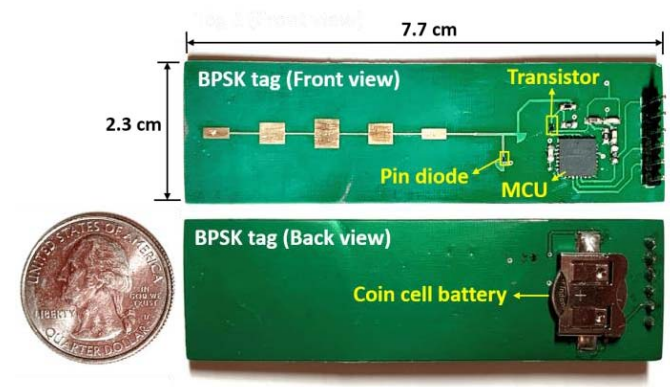


Fig. 5. Photographs of the fabricated BPSK tag.

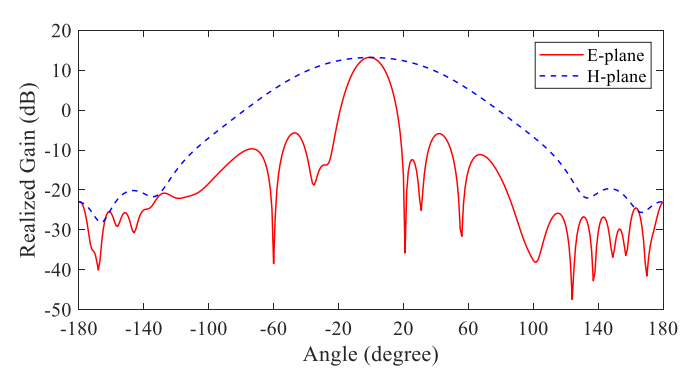


Fig. 6. Simulation result of the series-fed antenna at 24 GHz.

the circuit. In this state, the pin diode can be modeled as a high impedance that is in parallel with the RF open created by RS2 and the quarter-wave transformer. If the RF open is well designed, it will exhibit a much higher impedance compared with the pin diode at 0 V reverse bias condition. Therefore, the reflection coefficient will be highly dependent on the diode's isolation.

Photographs of the implemented tag are shown in Fig. 5. Two tags, named Tag 1 and Tag 2, were fabricated on a thin flexible substrate (CuClad 217). To switch between short and open circuit, a pin diode (MACOM MADP-000907-14020) is utilized. The modulation switching signal is generated by an on-board microcontroller (Microchip PIC18F24K42T-I). An output buffer (Toshiba SSM3J56ACT) and a bias resistor R_{bias} are added to drive the diode's current. A 3-V coin cell battery is mounted on the back side to supply the tag. The current consumption for each tag is 12 mA in the diode-ONstate and 0 mA in the diode-OFF-state. The power consumption is approximately 18 mW. A series-fed antenna was designed and used for both receiving and transmitting. Its simulation result is shown in Fig. 6. The simulated peak gain is 13 dB with a half-power beamwidth of 20° on E-plane and 80° on H-plane.

Simulations were carried out to evaluate the performance of the proposed tag architecture over the frequency range of 23.5–24.5 GHz. Electromagnetic (EM) structures were used to model the transmission lines and a manufacturer-provided S-parameter file for the desired bias conditions was applied to model the diode. The reflection coefficients of the fabricated

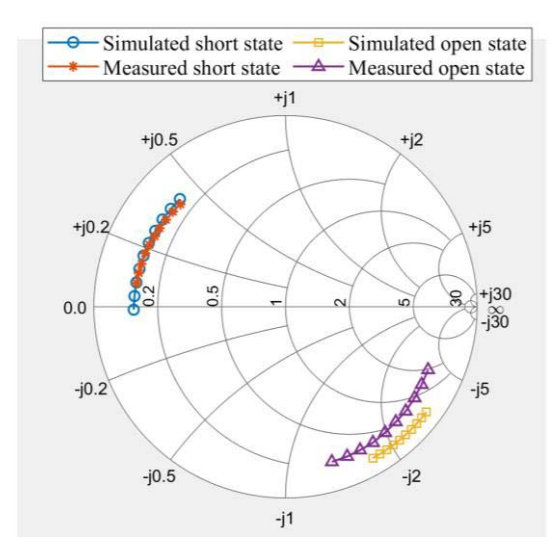


Fig. 7. Simulated and measured reflection coefficients for frequency range of 23.5–24.5 GHz. (a) Magnitudes. (b) Phases.

tag were measured with an Agilent 8722ES vector network analyzer (VNA). To interface with the VNA, the antenna of the tag was cutoff, a SubMiniature version A (SMA) connector was attached to the end of the microstrip line, and the introduced phase delay was removed during the calibration process. Comparisons between the tag's simulated and measured reflection coefficients are depicted in Fig. 7. For the short-circuit state at 24 GHz, the magnitudes of the simulated and measured reflection coefficients are 0.7875 and 0.7745, respectively; the corresponding phase results are -200.8° and -206.6° , respectively. For the open circuit state at 24 GHz, the simulated and measured magnitudes are 0.9167 and 0.8385, respectively, with the corresponding phases being -48.25° and -49.4° , respectively.

Overall, the measured and simulated reflection coefficients agree well. The variation in amplitudes compared with the ideal values can be explained by the nonidealities of the diode and transmission line losses and the small discrepancy between the simulated and measured phase values at the short state by the circuit's parasitic capacitances and fabrication errors (e.g., 125 μ m of microstrip length variation introduces 10° error in phase). The phase shift of around 49° from the ideal value of 0° for both simulated and measured phases at the open state is caused by the finite isolation of the diode. It should be noted that the small difference between the measured results and the ideal values does not affect the tag's overall performance, since on average 83% of the signal is reflected back from the tag to the radar. In addition, although the measured reflection coefficients amplitudes at the short and open states (i.e., 0.7745 and 0.8385) are different, they do not affect the range measurement because the range is calculated from the phase difference of the carrier responses. Because the two carrier frequencies are very close to each other, their reflection coefficients are assumed to be the same, i.e., independent of the carrier frequencies. Therefore, the tag introduces the same phase shift for the two carrier frequencies, which cancels out while calculating the difference between the phases from the f_1 and f_2 component.

TABLE I SPECIFICATIONS OF THE 24-GHz FSK RADAR

f_{sqr}	1.2 kHz		
f_{l}	23.8189 GHz		
f_2	23.8651 GHz		
Δf	46.2 MHz		
R_{max}	3.25 m		
Transmit power	15 dBm		
Antenna gain	20 dB		
Antenna beamwidth (E-plane)	45°		
Antenna beamwidth (H-plane)	38°		

Moreover, even though the measured phases (i.e., -206.6° and -49.4°) at the two states both shifted from the ideal values of -180° and 0° , the phase difference between them (i.e., 157.2°) is close to the desired 180°, which is more important than their absolute values for up-conversion purposes. Theoretically, any two phase shifts will generate two different voltage levels in the baseband signal. A phase difference of 180° between the two phase shifts is ideal because in this case, the voltage difference between the two voltage levels is maximized and a large modulation index is achieved. After FFT, the resulting modulation frequency peak will have a higher power level and higher SNR than a lower phase difference case. Though the achieved phase difference of 157.2° is less than the ideal value of 180° and hence resulting in a lower modulation index, it is sufficient to achieve a good modulation index and fulfill the desired up-conversion goal.

IV. EXPERIMENTS

For system level experiments, Tag 1 and Tag 2 were programed with a modulation frequency of $f_{m1} = 68.7$ Hz and $f_{m2} = 108.4$ Hz, respectively. A 24-GHz FSK radar (InnoSent IVS-162) equipped with two 4 × 2 patch antennas was used for the following experiments. A list of the radar specifications is provided in Table I. A 1.2-kHz square wave control frequency is generated by a function generator (Instek GFG-8210), which switches the transmit frequency between 23.8189 and 23.8651 GHz with a frequency shift of 46.2 MHz. The maximum unambiguous range is calculated according to (18) as 3.25 m. Both, the square wave and in-phase/quadrature (I/Q) channels, were recorded using National Instruments (NI) USB-6009. All the experiments were carried out in a residential indoor environment.

A. Single Tag Ranging

In the first experiment, the performance of each tag was evaluated at various locations from the radar. A photograph of the experimental setup is shown in Fig. 8(a). A wooden board was used as a mount support for Tag 1, which was then mounted on a tripod. Tag 1 was moved from 0.4 to 2.8 m in increments of 0.4 m. Three measurements of 0.5-s duration with sampling frequency of 15 kHz were recorded at each location. The square wave control signal was utilized to separate the f_1 and f_2 responses [25]. A segment of the I/Q channels of the separated f_2 responses recorded with Tag 1 at 0.4 m is shown in Fig. 8(b), where the BPSK modulation effect caused by the alternating phase shifts can be clearly observed.

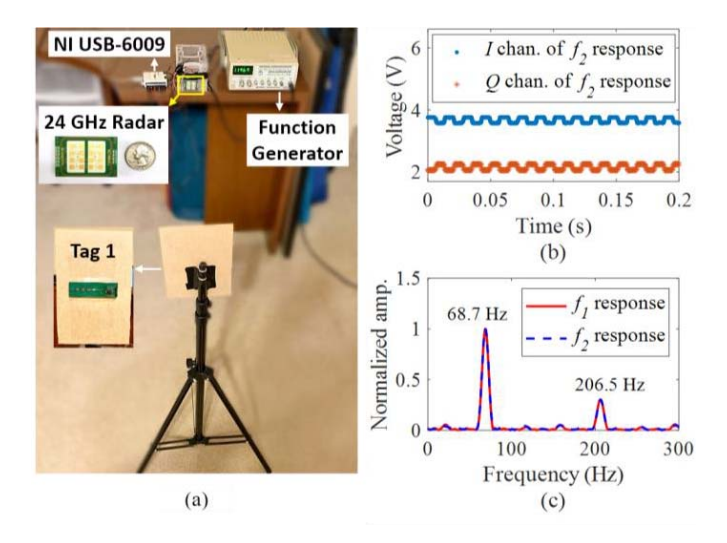


Fig. 8. (a) Photograph of the experimental setup of Tag 1 range measurement. (b) Segment of the separated f_2 responses recorded with Tag 1 at 0.4 m. (c) Corresponding spectra of (b).

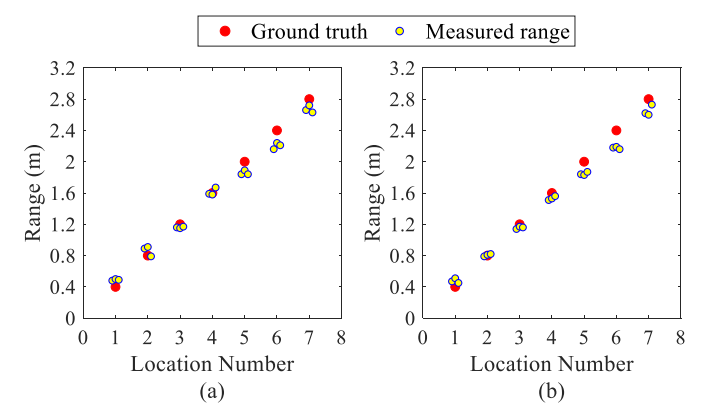


Fig. 9. Range estimation results of a single tag at various locations. (a) Tag 1. (b) Tag 2.

A 0.1-s FFT sliding window resulting in a 10-Hz frequency resolution was chosen with a 0.05-s sliding window step. Nine range estimations were thus obtained, and their average was used as final result for each measurement. As can be seen from the spectra in Fig. 8(c), of the separated baseband responses, the modulation frequency of Tag 1 and its third harmonic occur on both the f_1 and f_2 responses, which verifies the fundamental theory of BPSK tag-based range tracking. By comparing the phase difference between the modulation frequency pair, the range to the tag was estimated according to (10). The same experimental procedure and settings were implemented for Tag 2. The range estimation results of the two tags are plotted in Fig. 9(a) and (b), respectively. Approximately, 76% and 90% of the range results are within $\pm 10\%$ and $\pm 20\%$ of the ground truth for Tag 1; 86% and 95% of the range results are within $\pm 10\%$ and $\pm 20\%$ of the ground truth for Tag 2.

In a multipath environment, the signals reflected from many different directions and pathways combine constructively and destructively, leading to a phase-shifted signal response with respect to the direct path reflected signal, which can deteriorate the performance of phase-based range tracking radars [33].

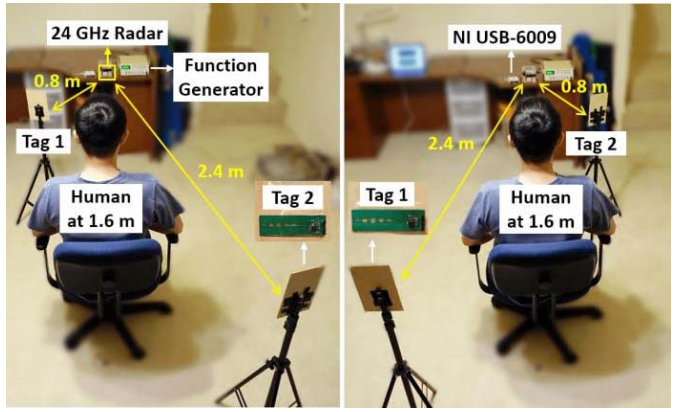


Fig. 10. Photographs of the experimental setup of concurrent multitag and a human target detection. The human target was seated at 1.6 m. (a) Tag 1 and Tag 2 were located at 0.8 and 2.4 m, respectively. (b) Tag 1 and Tag 2 were located at 2.4 and 0.8 m, respectively.

The multipath interference effect is determined by various factors, such as environment structure and antenna beamwidth. Therefore, the phenomenon that the two tags have a very similar measurement performance at the same location can be explained by multipath interference. While the application environment is difficult to control, narrow antenna beamwidth can effectively reduce the indirect reflections at the expense of a narrower field-of-view. Therefore, proper antenna beamwidth needs to be chosen for a given application, with consideration of the amount of multipath interference and acceptable field-of-view. In addition, signal equalization technique [34], [35] has potential to reduce multipath distortion, which will be explored in future work.

Though FFT was used in the baseband processing, given that the frequencies of the targets are known (i.e., tags' modulation frequencies), a more efficient processing approach is calculating the discrete Fourier transform (DFT) in the vicinity of those frequencies for a desired window size.

B. Concurrent Multitag and a Human Subject Detection

In the second experiment, a human subject along with the two tags was detected simultaneously. As demonstrated in Fig. 10(a) and (b), for experiment scenario 1, Tag 1 and Tag 2 were placed at 0.8 and 2.4 m, respectively; for scenario 2, Tag 1 was moved to 2.4 m and Tag 2 to 0.8 m. The untagged human target was seated at 1.6 m for both scenarios. Three measurements were recorded for each scenario with 15-kHz sampling frequency. A 60-s duration of the baseband signal was recorded for each measurement. FFT calculation was applied to the baseband data with 20-s window size, 5-s sliding step, Hamming window, and zero-padding for 260 s. Nine range estimations were calculated and the average of them was used as final range value for each measurement. As shown in Fig. 11(a) and (b), the range estimations of Tag 1 and Tag 2 were obtained from their own modulation frequency pairs (i.e., $f_{m1} = 68.7 \text{ Hz}$ and $f_{m2} = 108.4 \text{ Hz}$), while the range to the human target was acquired from the respiration frequency pair (i.e., $f_0 = 0.275 \text{ Hz}$) [25]. Measurement results can be found in Fig. 12. Again, acceptable range estimation was achieved with approximately 72% and 94% of the range results within $\pm 10\%$ and $\pm 20\%$ of the ground truth.

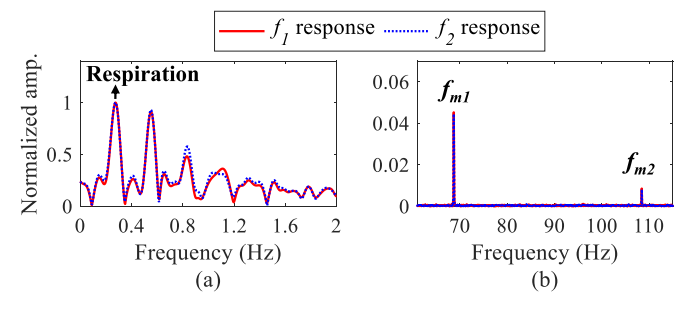


Fig. 11. Spectra when Tag 1, untagged human target, and Tag 2 are at 0.8, 1.6, and 2.4 m, respectively. (a) Low-frequency part of the spectra (0–2 Hz). (b) Spectra around the tags' modulation frequency.

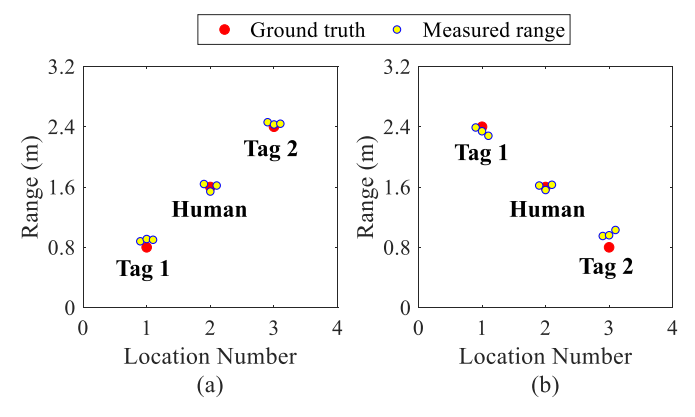


Fig. 12. Range estimation results of multiple tags and an untagged human subject. (a) Tag 1 and Tag 2 are at 0.8 and 2.4 m, respectively. (b) Tag 1 and Tag 2 are at 2.4 and 0.8 m, respectively.

Note that for practical implementations, parallel computing can be utilized to improve detection efficiency, where a long-time window can be used for the detection of respiration rate and a shorter time window can be used for the concurrent tag(s) detection. In addition, among rectangular window and Hamming window, the rectangular window provides better frequency resolution, while the Hamming window has higher dynamic range. Therefore, depending on the intended application, different window function can be chosen to achieve optimized signal processing results.

C. Multiple Tagged Human Subjects Detection

The purpose of the third experiment is to determine the ranges and vital signs from two tagged humans simultaneously. As illustrated in Fig. 13, the tags are attached to the chest of the two human subjects using nonelastic belts: Tag 1 attached to Subject 1 at 1.6 m; Tag 2 attached to Subject 2 at 0.8 m. Subject 2 also wore an elastic respiration belt as reference for the respiration measurement. A 60-s data segment was recorded with 10-kHz sampling frequency. Spectrogram calculation was performed on the respiration belt and baseband responses with a 20-s window length and 98% overlap rate. The spectrogram of the respiration belt data is plotted in Fig. 14(a), which clearly shows the respiration rate f_{02} . Its median normalized frequency is extracted and will be used as ground truth reference. Fig. 14(b) shows the spectrogram obtained from the f_1 responses, limited to 0–0.8 Hz. As illustrated, the respiration frequencies of the two subjects interfere with each other, causing them to be inseparable.

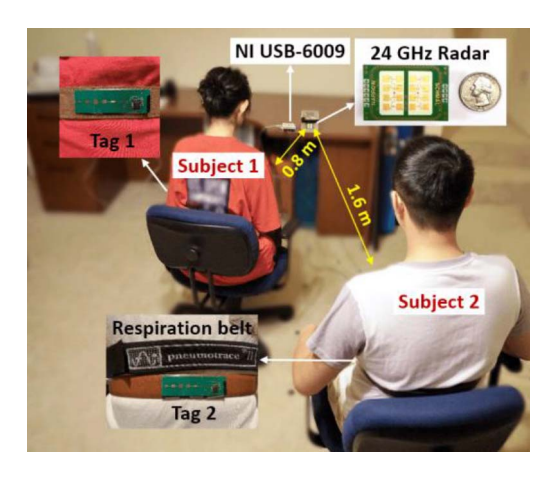


Fig. 13. Photograph of the experimental setup of multiple tagged human targets detection.

In comparison, distinct peaks related to the respiration rate f_{02} (i.e., $f_{m2} \pm f_{02}$) can be easily identified next to the modulation frequency f_{m2} of Tag 2 in Fig. 14(c), which coincide well with the reference. The respiration rate accuracy is calculated as the percentage of time that the detected rate is within 10% of the reference rate. The detection accuracy for both the f_{m2} + f_{02} and $f_{m2} - f_{02}$ frequencies is calculated to be 100%. Note that since the modulation frequencies have some variations with time, the measured instantaneous $f_{\rm m2}$ was used for accuracy calculation instead of a constant value of 108.4 Hz. The f_{m1} part of the f_1 responses spectrogram is presented in Fig. 14(d), where f_{m1} can be clearly located. However, Subject 1's respiration rate f_{01} (i.e., $f_{m1} \pm f_{01}$) cannot always be identified. Theoretically, since Subject 1 is closer to the radar than Subject 2, the f_{m1} and $f_{m1} \pm f_{01}$ frequencies should have higher power levels than the corresponding frequency components for Subject 2. The reason it is the opposite case can be caused by factors such as Subject 1's smaller chest wall movement and smaller illumination area due to misalignment of Tag 1 and radar. It was later discovered that the tags' movements were significantly constrained by the nonelastic belts that were used to attach the tags to the subjects, which also affect the vital signs sensing performance.

Range estimations for Subject 1 and Subject 2 were obtained from the f_{m1} pair and $f_{m2}/f_{m2}+f_{02}$ pair, respectively, as shown in Fig. 15. Calculation of the FFT on a 20-s sliding window with 5-s sliding step, Hamming window, and zero-padding for 85 s resulted in nine range calculations. The fact that the respiration frequencies of multiple targets were successfully recovered based on BPSK tags and the results from the f_{m2} pair and the $f_{m2}+f_{02}$ pair are very close to each other validates the theory of BPSK tag-based vital sign sensing and its corresponding range estimation.

To validate the aforementioned possible affecting factors for multivital-signs sensing, the second multihuman detection experiment with the same experiment setup was carried out, except that the nonelastic belts were replaced with elastic straps, Subject 1 was arranged to be more aligned with the radar line of sight, and Subject 1 wore the respiration belt instead. The obtained spectrogram plots are shown in Fig. 16. As can be seen, both subjects' respirations can

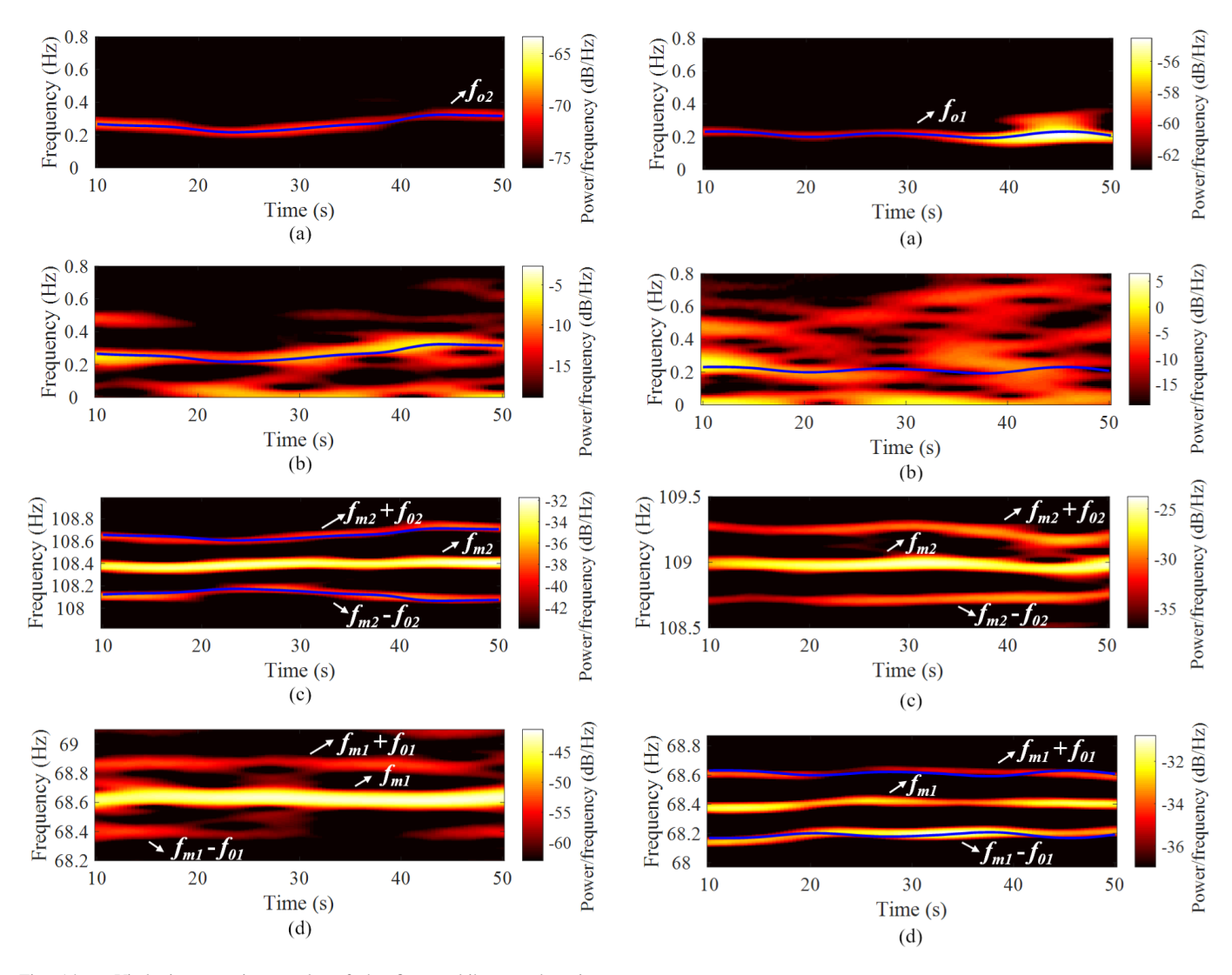


Fig. 14. Vital signs sensing results of the first multihuman detection experiment. (a) Spectrogram of the respiration belt data obtained from Subject 2. The extracted median frequency reference is shown in blue line. (b) Low-frequency part of the f_1 responses spectrogram (0–0.8 Hz) with the respiration reference obtained from (a). (c) f_{m2} part of the f_1 responses spectrogram with the respiration references obtained from (a). (d) f_{m1} part of the f_1 responses spectrogram.

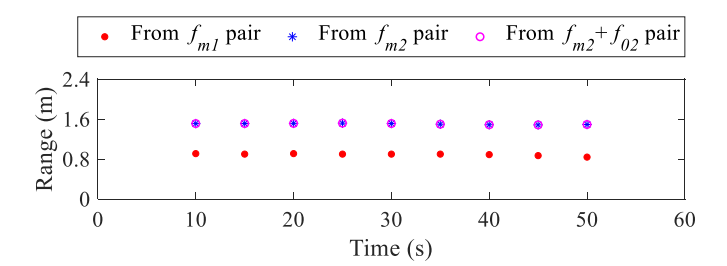


Fig. 15. Range estimation results of the first multihuman detection experiment (associated with Fig. 14).

be clearly identified; next, their modulation frequencies and Subject 1's respiration f_{01} (i.e., $f_{m1} \pm f_{01}$) agree with the reference. The detection accuracy for the $f_{m2} + f_{02}$ and $f_{m2} - f_{02}$ tones is calculated as 81% and 92%, respectively.

Comparing Fig. 16(c) and (d) with Fig. 14(c) and (d), it is shown that the power levels of the modulation frequencies

Fig. 16. Vital signs sensing results of the second multihuman detection experiment. (a) Spectrogram of the respiration belt data obtained from Subject 1. The extracted median frequency reference is shown in blue line. (b) Low-frequency part of the f_1 responses spectrogram (0–0.8 Hz) with the respiration reference obtained from (a). (c) f_{m2} part of the f_1 responses spectrogram. (d) f_{m1} part of the f_1 responses spectrogram with the respiration references obtained from (a).

and vital signs frequencies of both subjects are higher for the second experiment, confirming that the tags' movements in the first experiment were constrained by the nonelastic belts and the tags' movements in the second experiment were stronger due to the employment of elastic straps. Subject 1's associated frequency power levels are lower than that of Subject 2 for both experiments, despite that Subject 1 was located closer to the radar, proving that the reason is Subject 1's smaller breathing motion amplitude. The power level difference between Subject 1 and 2 was smaller for the second experiment when Subject 1 was closer to the radar line of sight, proving that the smaller illumination area due to the misalignment of Tag 1 and radar was a contributing factor for the previous poor respiration measurement.

The range estimation results of the second multihuman detection experiment are shown in Fig. 17. In comparison, the second range results have larger errors (about 24 cm for

Reference	[6]	[12]	[15]	[16]	This work
Radar type	Software defined radio (SDR)	Intermodulation/FSK	FMCW	SIL	FSK
Tag technology	Harmonic	Intermodulation	Sub-harmonic	SIL	Low-IF
Tag type	Passive	Passive	Active	Active	Active
Operating frequency	950 MHz/1.9 GHz	5.8 GHz	24 GHz/2.4 GHz	2.4 GHz	24 GHz
Frequency band occupation	2	1	2	1	1
Transmit power	>10 dBm	8 dBm	-10.7 dBm	5 dBm	15 dBm
Reported range	1.5 m	1 m	5 m	8 m	2.8 m
Multi-target detection reported	Yes	No	No	Yes	Yes
Multi-target detection technology	CDMA/TDMA	N/A	N/A	FDMA	Digital modulation
Range accuracy	mm range (multi-target)	<10% of ground truth (single target)	22.3 cm (single target)	10 cm (multi-target)	Around 20-30 cm (multi-target)
Vital sign sensing accuracy	Good	Good	N/A	Good	Good
Completely stationary target detection capability	Yes	No	Yes	No	Yes
Cost of radar	High	High	Moderate	Moderate	Moderate

TABLE II
PERFORMANCE COMPARISONS WITH RELATED STATE-OF-THE-ART RADARS IN LITERATURES

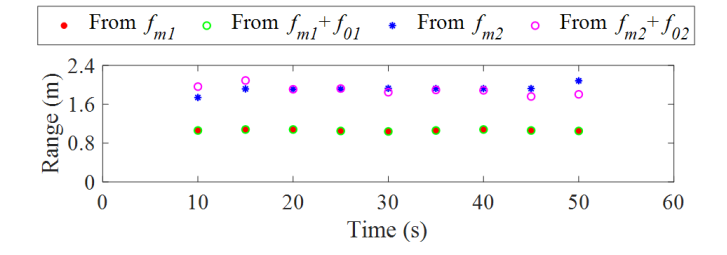


Fig. 17. Range estimation results of the second multihuman detection experiment (associated with Fig. 16).

Subject 1 and 31 cm for Subject 2) and standard deviations than the previous results shown in Fig. 15. Through experimentation, it is observed that random errors of 20–30 cm for multihuman detection are common, which are caused by multipath interference.

The nonideal vital signs sensing performance in the first multihuman detection experiment and the range estimation performance in the second experiment indicate that the detection system still has room for improvement to achieve a more robust multihuman detection. Nonetheless, the vital signs sensing and ranging performance demonstrate that the proposed system has potential to be utilized in various tracking scenarios.

V. ADVANTAGES AND LIMITATIONS

Table II compares the performance of the proposed work with related state-of-the-art customized RFID radar systems in literature. Although the passive tag-based nonlinear radar systems [6], [12] do not require a power source for the tag, their radar designs are more complicated and costly due to the nonlinear frequency operation compared with the proposed linear radar system. The work in [6] utilizes CDMA and TDMA for multitarget detection, bringing the benefits of better immunity to multipath interference and high range accuracy than the proposed system, at the expense of hardware

complexity and computation load. The active subharmonic tag system reported in [15] has comparable range accuracy as the proposed work, yet this subharmonic technology and the harmonic technology in [6] both occupy two frequency bands, which increase frequency band licensing cost. The active SIL tag technique reported in [16] shows better range accuracy for multitarget tracking than this work. However, the manually implemented FDMA protocol is less convenient and more complicated than the corresponding digital modulation scheme utilized in the proposed BPSK tag. In addition, since its range tracking is motion based, the SIL technique cannot track the range of completely stationary target. In summary, the proposed BPSK tag incorporated FSK radar system offers the advantages of simple radar architecture, single frequency band occupation, simple digital modulation, completely stationary target detection capability, and low cost, while the tradeoffs are active tag operation, sensitive to multipath interference, and moderate range accuracy.

The aforementioned experiments have demonstrated the ability of FSK radar to detect the respiration rates of single/multiple human subjects relying on BPSK tag(s) under controlled testing conditions. In other words, there are no random body movements present. However, during the acquisition of the vital signs in real-world applications, the subjects are likely to have random movements, such as moving hands, legs, and body, which may disrupt the desired vital signs information. Certain thresholds and features will have to be implemented in order to filter out the false alarms caused by the user-induced motion artifacts. Several random body movement cancellation techniques have also been proposed in the literature [36]–[38], which either require a complicated system architecture or signal processing approaches, all of which fall short to fully resolve the issue. Hence, this remains one of the critical challenges that prevents the radar-based vital signs sensing technology from being widely used. In addition, it should be noted that a long FFT window size (e.g., 20 s)

is required to obtain the low respiration frequency with good accuracy, which results in a low time resolution and needs to be considered for practical scenarios.

The proposed system relies on different BPSK tag modulation frequencies for multitarget identification and tracking. The number of tagged targets that the proposed system can detect is directly related to tag capacity, which is limited by the sampling frequency that the ADC can support. Higher sampling capability can accommodate higher modulation frequencies and larger number of modulation frequencies, at the expense of increased cost and computation load. Moreover, regarding mass production, those tags with identical frequencies must not be used in the same setting.

VI. CONCLUSION

A BPSK tag-based noncontact vital sign sensing and range tracking system has been demonstrated. The tag consists of simple microwave structures and readily available commercial off-the-shelf components, such as diode, transistor, and microcontroller, without the need for a mixer. Spectral analysis is performed to develop the tag-based vital sign sensing and ranging theories. Compared with the traditional FSK radar, the proposed BPSK tags enable the capability to detect completely stationary objects, multiple respirations, and ranges of multiple targets. Experimental results have verified the functionalities and demonstrated the potential for the proposed system to be utilized in various tracking scenarios.

REFERENCES

- [1] X. Jia, Q. Feng, T. Fan, and Q. Lei, "RFID technology and its applications in Internet of Things (IoT)," in *Proc. 2nd Int. Conf. Con*sum. Electron., Commun. Netw. (CECNet), Yichang, China, Apr. 2012, pp. 1282–1285.
- [2] M. Zhang, F. Sun, and X. Cheng, "Architecture of Internet of Things and its key technology integration based-on RFID," in *Proc. 5th Int. Symp. Comput. Intell. Design*, Hangzhou, China, Oct. 2012, pp. 294–297.
- [3] S. F. Khan, "Health care monitoring system in Internet of Things (IoT) by using RFID," in *Proc. 6th Int. Conf. Ind. Technol. Manage. (ICITM)*, Cambridge, U.K., Mar. 2017, pp. 198–204.
- [4] P. Gope, R. Amin, S. K. H. Islam, N. Kumar, and V. K. Bhalla, "Lightweight and privacy-preserving RFID authentication scheme for distributed IoT infrastructure with secure localization services for smart city environment," *Future Gener. Comput. Syst.*, vol. 83, pp. 629–637, Jun. 2018.
- [5] K. Fan, W. Jiang, H. Li, and Y. Yang, "Lightweight RFID protocol for medical privacy protection in IoT," *IEEE Trans. Ind. Informat.*, vol. 14, no. 4, pp. 1656–1665, Apr. 2018.
- [6] X. Hui and E. C. Kan, "Monitoring vital signs over multiplexed radio by near-field coherent sensing," *Nature Electron.*, vol. 1, no. 1, pp. 74–78, Nov. 2017.
- [7] C. Mandel, C. Schuster, B. Kubina, M. Schussler, and R. Jakoby, "Dual frequency selective multiple access with quasi-chipless/powerless RFID mixer tags," *IEEE Microw. Wireless Compon. Lett.*, vol. 24, no. 8, pp. 572–574, Aug. 2014.
- [8] K. A. Gallager, "Harmonic radar: Theory and applications to nonlinear target detection, tracking, imaging and classification," Ph.D. dissertation, Dept. Elect. Eng., Pennsylvania State Univ., State College, PA, USA, Dec. 2015.
- [9] A. Singh and V. M. Lubecke, "Respiratory monitoring and clutter rejection using a CW Doppler radar with passive RF tags," *IEEE Sensors J.*, vol. 12, no. 3, pp. 558–565, Mar. 2012.
- [10] S. Mondal and P. Chahal, "A passive harmonic RFID tag and interrogator development," *IEEE J. Radio Freq. Identificat.*, vol. 3, no. 2, pp. 98–107, Jun. 2019.
- [11] A. Mishra and C. Li, "A low power 5.8-GHz ISM-band intermodulation radar system for target motion discrimination," *IEEE Sensors J.*, vol. 19, no. 20, pp. 9206–9214, Oct. 2019.

- [12] A. Mishra, W. McDonnell, J. Wang, D. Rodriguez, and C. Li, "Intermodulation-based nonlinear smart health sensing of human vital signs and location," *IEEE Access*, vol. 7, pp. 158284–158295, 2019.
- [13] V. Viikari et al., "Technical solutions for automotive intermodulation radar for detecting vulnerable road users," in Proc. IEEE 69th Veh. Technol. Conf. (VTC Spring), Barcelona, Spain, Apr. 2009, pp. 1–5.
- [14] H. Gomes and N. B. Carvalho, "RFID for location proposes based on the intermodulation distortion," *Sensors Transducers*, vol. 106, no. 7, pp. 85–96, Jul. 2009.
- [15] N. El Agroudy, M. El-Shennawy, N. Joram, and F. Ellinger, "Design of a 24 GHz FMCW radar system based on sub-harmonic generation," *IET Radar, Sonar Navigat.*, vol. 12, no. 9, pp. 1052–1057, Sep. 2018.
- [16] F.-K. Wang, C.-H. Fang, T.-S. Horng, K.-C. Peng, J.-Y. Li, and C.-C. Chen, "Concurrent vital sign and position sensing of multiple individuals using self-injection-locked tags and injection-locked I/Q receivers with arctangent demodulation," *IEEE Trans. Microw. Theory Techn.*, vol. 61, no. 12, pp. 4689–4699, Dec. 2013.
- [17] A. Strobel, C. Carlowitz, R. Wolf, F. Ellinger, and M. Vossiek, "A millimeter-wave low-power active backscatter tag for FMCW radar systems," *IEEE Trans. Microw. Theory Techn.*, vol. 61, no. 5, pp. 1964–1972, May 2013.
- [18] Z. Peng et al., "A portable FMCW interferometry radar with programmable low-IF architecture for localization, ISAR imaging, and vital sign tracking," *IEEE Trans. Microw. Theory Techn.*, vol. 65, no. 4, pp. 1334–1344, Apr. 2017.
- [19] Z. Peng, L. Ran, and C. Li, "A K-band portable FMCW radar with beamforming array for short-range localization and vital-Doppler targets discrimination," *IEEE Trans. Microw. Theory Techn.*, vol. 65, no. 9, pp. 3443–3452, Sep. 2017.
- [20] C. Li et al., "A review on recent progress of portable short-range noncontact microwave radar systems," *IEEE Trans. Microw. Theory Techn.*, vol. 65, no. 5, pp. 1692–1706, May 2017.
- [21] L. Zhang, Y.-C. Liang, and M. Xiao, "Spectrum sharing for Internet of Things: A survey," *IEEE Wireless Commun.*, vol. 26, no. 3, pp. 132–139, Jun. 2019.
- [22] J. Wang, Z. Peng, and C. Li, "An efficient and extended range tracking method using a hybrid FSK-FMCW system," in *IEEE MTT-S Int. Microw. Symp. Dig.*, Chengdu, China, May 2018, pp. 1–4.
- [23] J. Wang and C. Li, "A human tracking and physiological monitoring FSK technology for single senior at home care," in *Proc. 40th Annu. Int. Conf. IEEE Eng. Med. Biol. Soc. (EMBC)*, Honolulu, HI, USA, Jul. 2018, pp. 4432–4435.
- [24] J. Wang, T. Karp, J. M. Muñoz-Ferreras, R. Gómez-García, and C. Li, "A spectrum-efficient FSK radar solution for stationary human subject localization based on vital sign signals," in *IEEE MTT-S Int. Microw. Symp. Dig.*, Boston, MA, USA, Jun. 2019, pp. 140–143.
- [25] J. Wang, T. Karp, J.-M. Munoz-Ferreras, R. Gomez-Garcia, and C. Li, "A spectrum-efficient FSK radar technology for range tracking of both moving and stationary human subjects," *IEEE Trans. Microw. Theory Techn.*, vol. 67, no. 12, pp. 5406–5416, Dec. 2019.
- [26] J. Wang, D. Nolte, K. Tanja, J. Muñoz-Ferreras, R. Gómez-García, and C. Li, "Trade-off on detection range and channel usage for moving target tracking using FSK radar," in *Proc. IEEE Topical Conf. Wireless Sens. Netw. (WiSNeT)*, San Antonio, TX, USA, Jan. 2020, pp. 38–41.
- [27] I. Mostafanezhad and O. Boric-Lubecke, "Benefits of coherent low-IF for vital signs monitoring using Doppler radar," *IEEE Trans. Microw. Theory Techn.*, vol. 62, no. 10, pp. 2481–2487, Oct. 2014.
- [28] I. Mostafanezhad, O. Boric-Lubecke, and V. Lubecke, "A coherent low IF receiver architecture for Doppler radar motion detector used in life signs monitoring," in *Proc. IEEE Radio Wireless Symp. (RWS)*, New Orleans, LA, USA, Jan. 2010, pp. 571–574.
- [29] X. Ma, Y. Wang, W. Song, X. You, J. Lin, and L. Li, "A 100-GHz double-sideband low-IF CW Doppler radar in 65-nm CMOS for mechanical vibration and biological vital sign detections," in *IEEE MTT-S Int. Microw. Symp. Dig.*, Boston, MA, USA, Jun. 2019, pp. 136–139.
- [30] A. D. Droitcour, O. Boric-Lubecke, V. M. Lubecke, J. Lin, and G. T. A. Kovac, "Range correlation and I/Q performance benefits in single-chip silicon Doppler radars for noncontact cardiopulmonary monitoring," *IEEE Trans. Microw. Theory Techn.*, vol. 52, no. 3, pp. 838–848, Mar. 2004.

- [31] C. Li, Y. Xiao, and J. Lin, "Experiment and spectral analysis of a low-power Ka-band heartbeat detector measuring from four sides of a human body," *IEEE Trans. Microw. Theory Techn.*, vol. 54, no. 12, pp. 4464–4471, Dec. 2006.
- [32] H. Zhang and K. Wu, "Three-frequency principle for automotive radar system," in *Proc. IEEE Radio Wireless Conf.*, Atlanta, GA, USA, Sep. 2004, pp. 315–318.
- [33] S. L. Wilson and B. D. Carlson, "Radar detection in multipath," *IEE Proc.-Radar, Sonar Navigat.*, vol. 146, no. 1, pp. 45–54, Feb. 1999.
- [34] C. A. Siller, "Multipath propagation," *IEEE Commun. Mag.*, vol. 22, no. 2, pp. 6–15, Feb. 1984.
- [35] S. U. H. Qureshi, "Adaptive equalization," *Proc. IEEE*, vol. 73, no. 9, pp. 1349–1387, Sep. 1985.
- [36] C. Li and J. Lin, "Random body movement cancellation in Doppler radar vital sign detection," *IEEE Trans. Microw. Theory Techn.*, vol. 56, no. 12, pp. 3143–3152, Dec. 2008.
- [37] M.-C. Tang, F.-K. Wang, and T.-S. Horng, "Single self-injection-locked radar with two antennas for monitoring vital signs with large body movement cancellation," *IEEE Trans. Microw. Theory Techn.*, vol. 65, no. 12, pp. 5324–5333, Dec. 2017.
- [38] I. Mostafanezhad, E. Yavari, O. Boric-Lubecke, V. M. Lubecke, and D. P. Mandic, "Cancellation of unwanted Doppler radar sensor motion using empirical mode decomposition," *IEEE Sensors J.*, vol. 13, no. 5, pp. 1897–1904, May 2013.



Jing Wang (Student Member, IEEE) received the B.S. degree in communication engineering from the Fujian University of Technology, Fuzhou, China, in 2015. She is currently pursuing the Ph.D. degree in electrical engineering at Texas Tech University, Lubbock, TX, USA.

Her current research interests include microwave circuits, wireless radio frequency (RF) sensors, and their biomedical applications.



Daniel Rodriguez (Graduate Student Member, IEEE) received the B.S. degree in electronics and telecommunication engineering from the Autonoma del Caribe University, Barranquilla, Colombia, in 2014, and the M.S. degree from the University of Puerto Rico, Mayaguez, PR, USA, in 2018. He is currently pursuing the Ph.D. degree in electrical engineering at Texas Tech University, Lubbock, TX, USA.

From 2013 to 2014, he worked at the School of Military Engineers, Bogota, Colombia, on seismic

prospection systems for buried explosive artifact detection. He also served as an Instructor during his time at this institution. His research interests include analog circuits, microwave circuits and systems, wireless sensors, and on-chip solar energy harvesting.

Mr. Rodriguez was awarded as an HSF Scholar (one of approximately 10 000 of the best and brightest Hispanic students in the country among all disciplines) in 2019. He received the IEEE MTT-S Graduate Fellowship Award in 2020, the IEEE Microwave Theory and Techniques Society First and Second Place Winner Award in the 2019 Adaptive relay transceiver and High-Sensitivity Motion Radar student design competitions, respectively, the JT and Margaret Talkington graduate fellowship in 2017, and the University of Puerto Rico honor tuition exemption in February 2016 and January 2017. He was five times member of the Autonoma del Caribe University Roll of honor (5 best GPA). He is an active Reviewer for the IEEE TRANSACTIONS ON MICROWAVE THEORY AND TECHNIQUES, IEEE JOURNAL OF ELECTROMAGNETICS, RADIO FREQUENCY (RF) AND MICROWAVES IN MEDICINE AND BIOLOGY, and the IEEE SENSORS JOURNAL.



Ashish Mishra (Student Member, IEEE) received the B.E. degree in electronics and telecommunication engineering from the University of Mumbai, Mumbai, India, in 2012, and the M.S. degree in electrical engineering from Texas Tech University, Lubbock, TX, USA, in 2016, where he is currently pursuing the Ph.D. degree in electrical engineering.

He was an Intern at Unknot.ID, Orlando, FL, USA, from February 2020 to August 2020. His current research interests include microwave circuits, wireless radio frequency (RF) sensors, and their biomedical applications.



Prateek Reddy Nallabolu (Graduate Student Member, IEEE) received the B.Tech. degree in electronics and communications engineering from Jawaharlal Nehru Technological University, Hyderabad, India, in 2016, and the M.S. degree in electrical engineering from Texas Tech University in 2018. He is currently pursuing the Ph.D. degree at Texas Tech University, Lubbock, TX, USA.

His research interests include microwave circuits, wireless radio frequency (RF) sensors, and their biomedical applications.



Tanja Karp (Senior Member, IEEE) received the Dipl.Ing. (M.S.E.E.) degree in electrical engineering and Dr.Ing. (Ph.D.) degree from the Hamburg University of Technology, Hamburg, Germany, in 1993 and 1997, respectively.

In 1997, she joined the Institute of Computer Engineering, Mannheim University, Mannheim, Germany, as a Senior Research and a Teaching Associate. From 1998 to 1999, she taught as a Guest Lecturer with the Institute for Microsystems Technology, Freiburg University, Freiburg, Germany.

From 2000 to 2006, she was an Assistant Professor with the Department of Electrical and Computer Engineering, Texas Tech University (TTU), Lubbock, TX, USA, where she is currently an Associate Professor. From 2016 to 2017, she was a U.S. Fulbright Scholar with the University of South Africa (UNISA), Pretoria, South Africa. She has organized several K-12 robotics programs to promote science, technology, engineering, and mathematics (STEM) careers. Her research interests include multirate signal processing, filter banks, multicarrier modulation, and engineering education.

Dr. Karp is a recipient of the IEEE/ASEE Harriet B. Rigas Award in 2012 and the President's Awards for Excellence in Science, Mathematics, Engineering Mentoring (PAESMEM), in 2016.



Changzhi Li (Senior Member, IEEE) received the B.S. degree in electrical engineering from Zhejiang University, Zhejiang, China, in 2004, and the Ph.D. degree in electrical engineering from the University of Florida, Gainesville, FL, USA, in 2009.

He is currently a Professor with Texas Tech University, Lubbock, TX, USA. His research interest is microwave/millimeter-wave technologies and their sensing applications.

Dr. Li was a recipient of the IEEE Microwave Theory and Techniques Society (MTT-S) Outstand-

ing Young Engineer Award, the IEEE Sensors Council Early Career Technical Achievement Award, the ASEE Frederick Emmons Terman Award, the IEEE-HKN Outstanding Young Professional Award, the NSF Faculty Early CAREER Award, and the IEEE MTT-S Graduate Fellowship Award. He is an Associate Editor of the IEEE TRANSACTIONS ON MICROWAVE THEORY AND TECHNIQUES and the IEEE JOURNAL OF ELECTROMAGNETICS, RADIO FREQUENCY (RF) AND MICROWAVES IN MEDICINE AND BIOLOGY.